Published in final edited form as:

J Magn Reson Imaging. 2022 May ; 55(5): 1440–1449. doi:10.1002/jmri.27935.

Perfusion and Permeability MRI Predicts Future Cavernous Angioma Hemorrhage and Growth

Je Yeong Sone, BA[1], **Nicholas Hobson, MSc**[1], **Abhinav Srinath, BA**[1], **Sharbel G. Romanos, BA**[1], **Ying Li, MD**[1], **Julián Carrión-Penagos, MD**[1], **Abdallah Shkoukani, MD**[1], **Agnieszka Stadnik, MSc**[1], **Kristina Piedad, RN BSN**[1], **Rhonda Lightle, BS**[1], **Thomas Moore, BS**[1], **Dorothy DeBiasse, BS**[1], **Dehua Bi, MSc**[1,2], **Robert Shenkar, PhD**[1], **Timothy Carroll, PhD**[3], **Yuan Ji, PhD**[2], **Romuald Girard, PhD**[1,*], **Issam A. Awad, MD**[1,*]

[1]Neurovascular Surgery Program, Department of Neurosurgery, University of Chicago Medicine and Biological Sciences, Chicago, IL, USA

[2]Department of Public Health Sciences, University of Chicago, Chicago, IL, USA

[3]Department of Diagnostic Radiology, University of Chicago Medicine and Biological Sciences, Chicago, IL, USA

Abstract

Background: Cerebral cavernous angioma (CA) is a capillary vasculopathy affecting more than a million Americans with a small fraction of cases demonstrating lesional bleed or growth with major clinical sequelae. Perfusion and permeability are fundamental features of CA pathophysiology, but their role as prognostic biomarkers is unclear.

Purpose: To investigate whether perfusion or permeability lesional descriptors derived from dynamic contrast-enhanced quantitative perfusion (DCEQP) MRI can predict subsequent lesional bleed/growth in the year following imaging.

Study Type: Single-site case-controlled study.

Subjects: 205 consecutively enrolled patients (63.4% female).

Field Strength/Sequence: 3-Tesla/T_1-mapping with contrast-enhanced dynamic 2D SPGR sequences.

Assessment: Prognostic associations with bleed/growth (present or absent) in the following year were assessed in 745 CA lesions evaluated by DCEQP in the 205 patients in relation to lesional descriptors calculated from permeability and perfusion maps. A subgroup of 30 cases also underwent peripheral blood collection at the time of DCEQP scans and assays of plasma levels of soluble CD14, IL-1β, VEGF, and soluble ROBO4 proteins, whose weighted combination had been previously reported in association with future CA bleeding.

Corresponding Author: Issam A. Awad, MD, MSc, FACS, MA (hon), Section of Neurosurgery, University of Chicago Medicine, 5841 S. Maryland, MC3026/Neurosurgery J341, Chicago, IL 60637 USA; Telephone +1 773-702-2123; Fax +1 773-702-3518; iawad@uchicago.edu.
*These senior authors contributed equally.

Statistical Tests: Mann-Whitney U-test for univariate analyses. Logistic regression models minimizing the Bayesian information criterion (BIC), testing sensitivity and specificity (receiver operating characteristic curves) of weighted combinations of parameters

Results: The best prognostic biomarker for lesional bleed or growth included brainstem lesion location, mean lesional permeability, and low-value perfusion cluster mean (BIC=201.5, sensitivity=77%, specificity=72%, $p<0.05$). Adding a previously published prognostic plasma protein biomarker improved the performance of the imaging model (sensitivity=100%, specificity=88%, $p<0.05$).

Data Conclusion: A combination of MRI-based descriptors reflecting higher lesional permeability and lower perfusion cluster may potentially predict future bleed/growth in CAs. The sensitivity and specificity of the prognostic imaging biomarker can be enhanced when combined with brainstem lesion location and a plasma protein biomarker of CA hemorrhage.

Keywords

Cavernous Angioma; Hemorrhage; Growth; Magnetic Resonance Imaging; Permeability; Perfusion

INTRODUCTION

Cerebral cavernous angiomas (CAs), also known as cerebral cavernous malformations (CCM), are clusters of abnormal capillaries with thin, dysregulated endothelial walls (1) affecting more than one million Americans (2). Most CA patients remain asymptomatic (1), but 25% carry a lifetime risk of CA-associated symptomatic hemorrhage (CASH) or lesional growth (3). The diagnosis of CASH requires evidence of lesional hemorrhage on MRI or computed tomography (CT), that is directly associated with attributable clinical symptoms including headaches, seizures and focal neurologic deficits (1,3). The annual risk for initial CASH is low, around 0.08% (3,4), however, the risk for recurrent hemorrhage increases up to 42% in the subsequent five years after an initial CASH diagnosis (2,3,5). In addition, subclinical hemorrhage and lesional growth (i.e., asymptomatic change) have been associated with prior and recurrent CASH (6). There is a need for a prognostic biomarker of CA bleeding and growth to help select high-risk cases for surgical interventions, particularly those with brainstem lesions carrying substantial surgical morbidity and a heavy economic burden of healthcare costs and disability (1). Repurposed drugs such as atorvastatin (clinicaltrials.gov: NCT02603328) (7) and propranolol (clinicaltrials.gov: NCT03589014) (8) are currently under investigation in clinical trials to reduce the risk of recurrent CASH. These and other novel drug interventions under development would benefit from a prognostic biomarker of CASH and asymptomatic changes by helping stratify higher risk patients in clinical trials.

The pathophysiology of CA is similar in familial/multifocal (20–30%) and sporadic/solitary (70–80%) lesions (9), related to germline and/or somatic mutations in three documented CA genes *CCM1*/*KRIT1, CCM2*/*Malcavernin*, and *CCM3*/*PDCD10*. The loss of function in the CA genes leads to aberrant upregulation of the RhoA kinase (ROCK) activity and disrupted brain-endothelial barrier integrity (10,11). These genetic and cellular dysfunctions may be

reflected as dysregulated vascular permeability (11) and perfusion (12) that can be measured by dynamic contrast-enhanced quantitative perfusion (DCEQP) MRI. In CA patients, the lesional permeability measured by DCEQP has been shown to be increased compared to normal brain parenchyma, regardless of the genotype (13). A longitudinal study has further reported an increase of the mean lesional permeability following a CA bleed/growth (14). Mean lesional permeability as assessed by DCEQP is being tested in a Trial Readiness initiative (clinicaltrials.gov: NCT03652181) as a potential monitoring biomarker of CASH (15,16). However, it is unclear whether lesional permeability measured using DCEQP may be a predictor of lesional bleed/growth (14).

Recently, a weighted combination, including lesional perfusion skewness and high perfusion cluster area measured by DCEQP, significantly distinguished a CA with symptomatic hemorrhage in the prior year. Additionally, a weighted combination of lesional perfusion entropy and skewness distinguished CA with symptomatic hemorrhage after 3 months, when hemorrhagic signatures would have disappeared from clinical MRI or CT imaging of the brain (17). Lesional permeability entropy, skewness and high-permeability cluster area also significantly distinguished a prior symptomatic hemorrhage but did not complement nor enhance the perfusion imaging models (17). These results supported laboratory studies linking hypoperfusion measured by low fluid shear stress with upregulated Rho kinase activity, inflammation, and signaling pathways associated with CA pathogenesis (12). A recent study in zebrafish also suggested that blood flow may be a crucial factor in CA pathogenesis (8).

In this study, we aimed to investigate whether CA lesional permeability and perfusion descriptors measured by DCEQP can predict future bleed/growth within a year after imaging. We additionally hypothesized that combinations of permeability and perfusion descriptors can complement and/or enhance clinical features and a plasma biomarker comprising levels of soluble CD14, IL-1β, VEGF, and soluble ROBO4 proteins, whose weighted combination had been previously reported in association with future CA bleed/growth (18).

MATERIALS AND METHODS

Study Participants

All enrolled patients provided written informed consent which adhered to the Declaration of Helsinki. This study was approved by the Institutional Review Board (IRB) (Study No. 12–0204). The ethical principles which guided the IRB were in accordance with The Belmont Report and the Federal Policy for the Protection of Human Subjects (56 FR 28003).

In this case-controlled study, 205 consecutive CA patients (63.4% female) were enrolled and underwent a DCEQP research MRI sequence in conjunction with clinical MRI of the brain between July 2012 and December 2019 at a single referral center. The research DCEQP sequence has undergone inter-observer validation (13,15). All patients underwent follow-up clinical assessment and MRI of the brain one year after enrollment and the DCEQP assessment, or sooner if they developed new symptoms. Baseline and follow-up clinical imaging sequences included conventional pre- and post-contrast MRI of the brain

as widely deployed clinically, and as recommended in evidence-based guidelines for clinical management of CAs (2).

Assessments of lesion size at enrollment and follow-up were performed by two investigators with more than 5 years experience in CA imaging (NH, RG) and adjudicated by senior clinician (IAA). Any bleed and expansion were further adjudicated in reference to formal clinical neuroradiologist read. Patients who had prior partial/complete CA resection or brain irradiation were excluded. A subset of 30 patients also underwent blood collection for plasma biomarker assays at the time of DCEQP.

Classification of CA Lesions and Follow-up Assessments

CA lesions were included in the analyses if the maximum diameter was ≥5 mm including the hemosiderin ring on axial T_2-weighted MRI sequence, and were covered by the DCEQP imaging data acquisition (see details below). Maximum lesion diameter was measured manually using the clinical MRI instrument software, and the lesion diameter threshold corresponded to “large lesion” diameter threshold in ongoing clinical research studies meant to exclude smaller lesions or hemorrhagic microangiopathies with unknown clinical significance (2,6,7,13,14,16,17). Each CA lesion was classified as its own observation point, and was categorized as familial/multifocal if there were multiple CAs in the brain on magnetic resonance susceptibility weighted imaging (SWI, GRE with repetition time/ echo time 49/40 milliseconds, axial plane, flip angle 15 degrees, field of view 230 X 200 mm, matrix 256 X 177, section thickness 2 mm) (19), a documented *CCM1*, *CCM2*, or *CCM3* germline mutation on genetic testing, and/or first-degree relative with CA history. Lesions were categorized as sporadic/solitary if they presented a single CA lesion on SWI or a cluster of CAs associated with a developmental venous anomaly. Lesions were also categorized by brainstem location (yes or no), and prior symptomatic hemorrhage (yes or no) in the year preceding the DCEQP imaging (17).

CAs showing acute or subacute bleeding on follow-up CT or clinical MRI (including evidence of new fluid-attenuated inversion recovery (FLAIR) signal on MRI, and/or lesion expansion in any diameter by ≥3 mm on comparable T_1- or T_2-weighted clinical MRI sequences (2,6,14,16,20) were categorized as bleed/growth for further prognostic analyses. The ≥3 mm threshold on comparable T_1- or T_2-weighted MRI was previously used in analysis of subclinical changes in CAs (6) and is meant to exclude insignificant changes and those within errors of manual measurement on non-research MRI scans. Each CA lesion’s clinical categorization was adjudicated and classified by clinical team members reviewing the medical record and clinical imaging, blinded to the DCEQP research imaging data.

Imaging Acquisition and Postprocessing

Research and clinical imaging scans were acquired upon patient enrollment, using a 3.0-Tesla scanner with MultiTransmit Parallel RF Transmission Technology, Quasar Dual Gradient System, and 32-Channel Architecture (Achieva, Philips, Cambridge, MA, USA). Details of the imaging protocol and DCEQP sequences as applied to CA imaging have been published previously (13–15,21,22). Briefly, The DCEQP protocol consisted of three components that are run in succession: 1) arterial input function (AIF) Localizer, 2) a T1

map, and 3) dynamic contrast-enhanced scan. For AIF Localizer, a 3D time-of-flight image is acquired at the level of the pons to cover the internal carotid arteries. The reconstructed maximum intensity projection (MIP) images in both the coronal and sagittal planes are used to prescribe the slice orthogonal to the ascending portion of the carotid artery for the AIF. Then a 2D saturation recovery gradient recalled sequence (SRGR) for an initial T1 measurement. Unlike conventional MRI scans, the DCEQP technique requires the selection of up to five axial slices for desired regions of interest because of limited time for dynamic imaging after contrast administration (21,22). The prototypical acquisition parameters used for both the T1 mapping and dynamic sequence were TE = 1.9 msec, TR = 3.9 msec, flip angle = 30, FOV = 230 X 182 mm^2, slice thickness = 8 mm, matrix size = 96 X 61, SENSE factor = 2, centric order phase encoding. The T1 mapping was performed by varying the time delay (TD) following the nonselective inversion pulse, for TD values of 120 msec, 300 msec, 600 msec, 1 sec, 2 sec, 4 sec, and 10 sec, then fitting the inversion recovery signal equation to the measured signal values for each voxel. The dynamic sequence used the shortest delay time, 120 msec, and consisted of 250 2D image acquisitions for each of up to five slices, selected to maximize coverage of the index CA in sporadic/solitary cases or as many CA lesions as possible in familial/multifocal cases (13–15,21,22), with a total of up to 1250 images and total scan duration of up to 5:04 minutes. The same base sequence was used for both the T1-weighted mapping and the dynamic series. MultiHance (gadobenate dimeglumine, Bracco Diagnotics, Inc., Monroe Township, NJ, USA) is administered (0.1 mMol/kg), using a computer-controlled power injector through an 18-gauge catheter placed in the antecubital vein. Injection and saline flush (15 ml) should both be at 4.0 ml/sec and initiated after the 9th measurement (12 seconds after scan initiation) of the dynamic sequence. Since the scan was often performed as a part of routine clinical care brain MRI with and without contrast, one half of the contrast agent will be used for the permeability scan. After the permeability scan is complete, the remaining half-dose (i.e. an additional 0.1 mmol/kg by body weight, for a total dose of 0.2 mml/kg) is injected and routine post-contrast clinical MRI can be completed. Clinical MRI implemented brain imaging sequences before and after contrast administration, per sequences recommended in guidelines for clinical diagnosis and follow-up of CAs (2).

Regions of interest (ROIs) were selected using Image J software (Bethesda, MD, USA: US National Institutes of Health) on T2-weighted images acquired in the same orientation and immediately before the T1-weighted images. Lesional ROIs included the entire CA lesion, including surrounding hypo-intense “hemosiderin ring,” as seen on T2-weighted co-axial images. The DCEQP data were postprocessed into permeability and perfusion maps using pipelines implemented in MATLAB (MathWorks, Natick, MA) (14). The previously published processing technique (21,22) allows the simultaneous computation of permeability (mL/100g/min) and perfusion (mL/100g/min) index maps corresponding to respective pixels on matched axial magnetic resonance images. See further information on image segmentation and postprocessing protocols is presented in the Supplementary Materials and Methods.

Thirteen permeability and perfusion lesional descriptors were calculated using MATLAB (MathWorks) and included mean, median, upper and lower terciles, coefficient of variation (CV), skewness, kurtosis, entropy, lesion area, high-value cluster mean, high-value cluster

area, low-value cluster mean, and low-value cluster area (Definitions and equations for these descriptors are presented in Supplementary Table 1). High- or low-value cluster areas were defined as regions of DCEQP maps with largest CA diameter in which all values were ≥1 standard deviation (SD) greater than or less than the mean, respectively.

Blood Collection and Plasma Protein Assays

Blood collection protocols, plasma processing and freeze-storage, subsequent ELISA assays of four plasma proteins (soluble CD14, IL-1β, VEGF, and soluble ROBO4), and their weighted combination in a canonical prognostic biomarker have been published previously (18). Methods are summarized in the Supplementary Materials and Methods.

Statistical Analyses and Bayesian Modeling

Difference in demographics between CA lesions with and without bleed/growth within a year after DCEQP imaging were assessed with χ^2-test or Fisher's exact test. Differences in values of the permeability and perfusion descriptors of CAs with versus without bleed/growth within a year after imaging were compared using Mann-Whitney U-test. Outliers with absolute studentized residual values of 3 or greater were excluded. Logistic regression $ln\left(\frac{P}{1-P}\right) = \sum_{i=1}^{n} \beta_i x_i + \beta_0$ was implemented to conduct multivariate analyses and develop the weighted prognostic combination models. Coefficients of models were reported with 95% confidence intervals (CIs). McFadden R^2 was used to measure variance in the data explained by each respective model (23). The best weighted combinations of non-correlated permeability and perfusion descriptors showing prognostic associations following exploratory univariate analyses (p<0.1) and demographics (age, sex, sporadic/familial, brainstem lesion location) were selected by minimizing the Bayesian information criterion (BIC) (24). The canonical biomarker scores were calculated from the logistic regression models as the predicted probability values and compared between CAs with and without bleed/growth using Mann-Whitney U-test. Then, the receiver operating characteristic (ROC) curves, areas under the curves (AUCs), and optimal sensitivity and specificity values were calculated (25). The ROC curves were compared using the DeLong method (26), from which the p-values were false-discovery rate (FDR)-corrected with the Benjamini and Hochberg method (27).

Finally, a previously derived and validated prognostic plasma CASH biomarker (with weighted combinations of the plasma levels of four proteins CD14, IL-1β, VEGF, and soluble ROBO4) (18) was assessed whether it can enhance the associations of the weighted combination model of permeability and perfusion imaging. In these integrative analyses, the canonical plasma biomarker score was incorporated as a covariate in the imaging models. For internal validation of the integrated model, Monte Carlo simulations were then conducted in 1000-fold increased populations (28). Statistical analyses were conducted with Prism v7.0 (GraphPad, San Diego, CA), SPSS v22.0 (IBM, Armonk, NY), and the R statistical framework (v4.1, R Foundation for Statistical Computing, https://www.r-project.org/). *For more information on material and methods refer to* Supplementary Information. The p-values were classified as statistically significant at α<0.05 and as having a trend at α<0.1.

RESULTS

Representation of MRI Sequences and the Permeability and Perfusion Descriptors

The representative axial T_2-weighted and T_1-weighted DCEQP MRI scans depicted the segmented lesional ROIs (Figure 1) that were utilized to acquire the 13 perfusion and 13 permeability descriptors (Figure 2).

Classification of CA Lesions

Among the 745 CAs with DCEQP data, 23 experienced bleed/growth (12 lesions with symptomatic hemorrhage and 11 with subclinical change) within a year following DCEQP MRI (Figure 3; Table 1; **please refer to** Supplementary Results **for patient demographics and valid DCEQP acquisition**). A significantly higher proportion of brainstem CAs were observed in the cohort of lesions that experienced bleed/growth within a year after imaging (Table 1). No other demographic, including age (p=0.34), sex (p=0.82), ethnicity/race (p=0.86), sporadic phenotype (p=0.11), genotype (p=0.92), and prior history of symptomatic hemorrhage (p=0.74), was significantly different between CAs with versus without bleed/growth.

The Best Prognostic Biomarker of CA with Lesional Bleed/Growth within a Year after Imaging Was a Combination of Permeability and Perfusion Lesional Descriptor

In CAs with compared to without bleed/growth, respectively, univariate comparisons showed significantly greater values of high-perfusion cluster mean (median [interquartile range]=72.2 [36.2–142.3] vs. 47.9 [30.4–74.5]) and perfusion skewness (1.4 [0.7–2.5] vs. 1.0 [0.4–1.6]), along with decreased low-perfusion cluster mean (6.2 [0.0–12.9] vs. 10.6 [5.2–16.6]) and perfusion CV (1.6 [1.1–2.4] vs. 2.3 [1.6–3.3]) in CAs with bleed/growth within a year after imaging compared to CAs which showed no evidence of bleed/growth (Figure 4). Trends toward higher permeability values of mean (0.4 [0.2–0.6] vs. 0.3 [0.1–0.5], p=0.078), upper tercile (0.6 [0.3–0.9] vs. 0.4 [0.2–0.6], p=0.065), and high-permeability cluster mean (0.9 [0.5–1.2] vs. 0.6 [0.4–1.0], p=0.063) were also observed in the cohort of lesions that experienced bleed/growth within a year following imaging compared to lesions without bleed/growth, respectively.

Subsequent Bayesian model selection showed that the most significant prognostic model of CAs with bleed/growth within a year after imaging (BIC=201.5, McFadden R^2=0.12) was a combination of brainstem lesion location, mean permeability, and low-perfusion cluster mean (all covariates p<0.05; Figure 5a, Supplementary Table 4):

$$\ln\left(\frac{P}{1-P}\right) = 1.5[\pm 1.0](Brainstem) + 1.07[\pm 0.7]\,(Mean\ Permeability) \\ -0.08[\pm 0.06](Low\ Perfusion\ Cluster\ Mean) - 3.5[\pm 0.8]$$

This model showed significantly higher median canonical scores in CAs with lesional bleed/growth and predicted bleed/growth with 77% sensitivity and 72% specificity (AUC=80%) (Figure 5b–c). The prognostic model predicted bleed/growth significantly better than mean permeability (AUC=65%) and low-perfusion cluster mean (AUC=67%), while the latter two individual descriptors did not significantly differ in performance (p=0.79, FDR-corrected).

Combining the Best Prognostic DCEQP Imaging Biomarker with a Published Prognostic Plasma Protein Biomarker Enhanced the Prognostic Sensitivity and Specificity

In the integrative analysis within a subset of 30 CA patients with both plasma and DCEQP imaging data, including 5 who experienced lesional bleed/growth within a year after imaging, the integrated weighted combination significantly predicted lesional bleed/growth with 100% sensitivity and 88% specificity (AUC=94%). Despite having higher sensitivity and specificity, this combined model did not significantly outperform the DCEQP imaging model (80% sensitivity, 79% specificity, AUC=76%; p=0.39, FDR-corrected) or the plasma biomarker individually (80% sensitivity, 92% specificity, AUC=88%; p=0.49, FDR-corrected) (Figure 6a–b). However, the Monte Carlo simulation showed that the integrated biomarker (AUC=93%) significantly outperformed each of the DCEQP imaging model (AUC=68%) and plasma biomarker model alone (AUC=89%) (Supplementary Figure 4).

DISCUSSION

We have shown that a weighted combination of increased mean permeability (i.e., vascular leak) and low perfusion cluster (i.e., a focal area of decreased lesional blood flow) assessed by DCEQP imaging, in addition to brainstem lesion location, may potentially predict CA lesional bleed/growth within a year following the imaging acquisition. Additionally, an integrative weighted model combining the DCEQP imaging data and a published prognostic plasma biomarker of lesional bleeding and growth (with weighted combined levels of four proteins CD14, IL-1β, VEGF, and soluble ROBO4) (18) enhanced the prognostic associations compared to permeability and perfusion imaging or the plasma protein biomarker alone.

A previous report identified that features reflecting inhomogeneous and dysregulated perfusion could best diagnose CASH (17). Our current study now suggests that increased permeability and decreased perfusion cluster may predict future lesional bleed/growth. This prognostic model is consistent with the existing knowledge on CA disease, including hyperpermeability's longitudinal association with CA bleed/growth (14). Low perfusion in the prognostic model is also consistent with a recent study showing that aspirin and statin therapies aimed at attenuating disrupted blood flow were associated with lower odds of CA hemorrhage (29). Finally, the DCEQP lesional imaging descriptors and proteins of the plasma biomarker (18,30) may reflect complementary biological mechanisms. Permeability and perfusion descriptors of the prognostic model may reflect the dysregulated angiogenesis and angioarchitecture of CA disease modulated by vascular endothelial growth factor (31,32) and its functionally related proteins (33).

The previous diagnostic study by Sone *et al.* (17) and our prognostic results herein both suggest that dysregulated perfusion and permeability may reflect pathophysiological changes of CA disease before and after bleed/growth. Ultimately, the diagnostic (17) and prognostic biomarkers have complementary contexts of use in the clinical management of hemorrhagic activity in CA patients. The diagnostic biomarker would allow for the identification of CASH patients with delayed or ambiguous presentation who may be candidates for surgical resection, by confirming that the lesion had bled previously, or enrollment in trials of novel therapies in CASH lesions (2,3,5,34). The prognostic

biomarker would allow for the detection of lesions at high risk for future bleed/growth, thus facilitating their consideration of proactive neurosurgical intervention if the lesion is surgically accessible, at low risk, or by stratifying higher risk cases in future clinical trials (2,6,34).

Among the 23 cases in this series with subsequent hemorrhage/growth (12 symptomatic, and 11 subclinical), 8 (34.8%) underwent surgical intervention (6 for symptomatic hemorrhage and 2 for subclinical change). In a previous study, patients with solitary lesion and subclinical growth or bleed were also more likely to undergo lesion resection (6). If the prognostic biomarkers described herein are validated in multisite populations and clinically accredited, they might motivate closer clinical surveillance or proactive neurosurgical intervention for accessible lesions destined to bleed. With emergence of novel therapies for the prevention of CASH, prognostic biomarkers such as those shown herein might allow stratification of higher risk cases for trials of these interventions.

Clinical features identified in the prognostic model were consistent with the existing knowledge on the cerebrovasculature and CA disease. It is possible that the higher odds of bleed/growth in brainstem lesions may suggest differential biological mechanisms predisposing lesions in the brainstem to bleed/growth. The heterogeneity of the blood-brain barrier throughout different brain regions, including the brainstem (35), may have contributed to this finding. The exclusion of sporadic/familial genotype from the prognostic model is also consistent with prior findings that sporadic/familial CAs have similar permeability (13) and pathophysiology (9). Another important clinical feature that was excluded from the integrated model was a prior history of symptomatic hemorrhage (6). This exclusion may be due to the possibility that prior bleed and dysregulated lesional perfusion and permeability may not be independent events. It is important that future multisite studies include sufficiently large cohorts to further investigate potentially differential biological risks and specific model applicability in subcohorts with brainstem lesion location, sporadic/familial genotypes, age, sex, and prior history of hemorrhage. If validated in independent multi-site cohorts, the results herein can help with the practical management of CAs by selecting high-risk cases for closer surveillance, for potentially morbid and costly surgical interventions (2), and for case stratification in clinical trials of novel interventions.

Limitations

Prospective symptomatic and subclinical bleeding and growth in the following year after DCEQP were combined into a single group due to the small number of cases with relevant events, and we did not investigate the model applicability at different time points within and beyond one year of follow-up. There is a close association between subclinical changes and prior and future CASH (6), but they may be reflected by distinct biomarkers if investigated separately. The higher odds of bleed/growth in brainstem lesions may also have reflected a detection bias. As the brainstem is an eloquent structure which may trigger observable symptoms after only a minor bleed/growth (2), subjects with brainstem bleed/growth may be more likely to attend a clinical visit and thus enroll in CA studies.

Additionally, it is possible that the prior history of symptomatic hemorrhage as a clinical feature may not have survived the Bayesian model selection due to a small sample of

previously bled lesions with DCEQP data and future follow-up, limiting the prognostic associations. Other limitations include low statistical power in the subcohorts examining the combination of DCEQP and plasma biomarkers. Prospective validation of the imaging biomarker in an independent cohort and at multiple sites remains to be assessed. This will be facilitated by recent multi-site and multi-instrument validations of DCEQP in CA (15).

The array of selected DCEQP descriptors may also have biased or limited the prognostic associations between the biomarkers and lesional bleed/growth. Supervised machine learning (36,37) and deep learning algorithms (38) in future studies may be used to identify permeability and perfusion descriptors and models which may be more reflective of conditions predisposing the CA lesional hemorrhage or growth.

Conclusions

The first implication of our results is the generation of mechanistic hypotheses about the roles of perfusion, permeability, and circulating blood biologic parameters in future CA bleeding and growth. This preliminary study also establishes feasibility and proof of concept in assessing DCEQP imaging as part of a panel of candidate biomarkers to predict CA bleed or growth. The enhanced performance of the combined biomarker of permeability and perfusion imaging and plasma proteins suggests that an integrative approach may be important to characterize lesion biology.

Supplementary Material

Refer to Web version on PubMed Central for supplementary material.

Acknowledgments and Grant Support:

This work was supported by grants from the NIH (R21NS087328, 5U01NS104157-02, 1R01NS107887-01), William and Judith Davis Fund in Neurovascular Research to IAA, by the Safadi Translational Fellowship to RG, and the Burroughs Wellcome Fund and the University of Chicago Pritzker School of Medicine to JYS. Funding sources played no role in the formulation of research questions nor the interpretation of results.

REFERENCES

1. Awad IA, Polster SP. Cavernous angiomas: deconstructing a neurosurgical disease. J Neurosurg 2019;131:1–13. [PubMed: 31261134]
2. Akers A, Al-Shahi Salman R, Awad IA, et al. Synopsis of guidelines for the clinical management of cerebral cavernous malformations: Consensus recommendations based on systematic literature review by the Angioma Alliance Scientific Advisory Board Clinical Experts Panel. Neurosurgery 2017;80:665–680. [PubMed: 28387823]
3. Al-Shahi Salman R, Hall JM, Horne MA, et al. Untreated clinical course of cerebral cavernous malformations: a prospective, population-based cohort study. Lancet Neurol 2012;11:217–224. [PubMed: 22297119]
4. Moore SA, Brown RD Jr., Christianson TJ, Flemming KD. Long-term natural history of incidentally discovered cavernous malformations in a single-center cohort. J Neurosurg 2014;120:1188–1192. [PubMed: 24628608]
5. Horne MA, Flemming KD, Su IC, et al. Clinical course of untreated cerebral cavernous malformations: a meta-analysis of individual patient data. Lancet Neurol 2016;15:166–173. [PubMed: 26654287]

6. Carrion-Penagos J, Zeineddine HA, Polster SP, et al. Subclinical imaging changes in cerebral cavernous angiomas during prospective surveillance. J Neurosurg 2020;134:1147–1154. [PubMed: 32244216]
7. Polster SP, Stadnik A, Akers AL, et al. Atorvastatin treatment of cavernous angiomas with symptomatic hemorrhage exploratory proof of concept (AT CASH EPOC) trial. Neurosurgery 2019;85:843–853. [PubMed: 30476251]
8. Li W, Shenkar R, Detter MR, et al. Propranolol inhibits cavernous vascular malformations by beta1 adrenergic receptor antagonism in animal models. J Clin Invest 2020;131:e144893. doi: 144810.141172/JCI144893.
9. McDonald DA, Shi C, Shenkar R, et al. Lesions from patients with sporadic cerebral cavernous malformations harbor somatic mutations in the CCM genes: evidence for a common biochemical pathway for CCM pathogenesis. Hum Mol Genet 2014;23:4357–4370. [PubMed: 24698976]
10. Stamatovic SM, Sladojevic N, Keep RF, Andjelkovic AV. PDCD10 (CCM3) regulates brain endothelial barrier integrity in cerebral cavernous malformation type 3: role of CCM3-ERK1/2-cortactin cross-talk. Acta Neuropathol 2015;130:731–750. [PubMed: 26385474]
11. Stockton RA, Shenkar R, Awad IA, Ginsberg MH. Cerebral cavernous malformations proteins inhibit Rho kinase to stabilize vascular integrity. J Exp Med 2010;207:881–896. [PubMed: 20308363]
12. Li J, Zhao Y, Coleman P, et al. Low fluid shear stress conditions contribute to activation of cerebral cavernous malformation signalling pathways. Biochim Biophys Acta Mol Basis Dis 2019;1865:165519. doi: 10.1016/j.bbadis.2019.07.013.
13. Mikati AG, Khanna O, Zhang L, et al. Vascular permeability in cerebral cavernous malformations. J Cereb Blood Flow Metab 2015;35:1632–1639. [PubMed: 25966944]
14. Girard R, Fam MD, Zeineddine HA, et al. Vascular permeability and iron deposition biomarkers in longitudinal follow-up of cerebral cavernous malformations. J Neurosurg 2017;127:102–110. [PubMed: 27494817]
15. Hobson N, Polster SP, Cao Y, et al. Phantom validation of quantitative susceptibility and dynamic contrast-enhanced permeability MR sequences across instruments and sites. J Magn Reson Imaging 2019;51:1192–1199. [PubMed: 31515878]
16. Polster SP, Cao Y, Carroll T, et al. Trial readiness in cavernous angiomas with symptomatic hemorrhage (CASH). Neurosurgery 2019;84:954–964. [PubMed: 29660039]
17. Sone JY, Li Y, Hobson N, et al. Perfusion and Permeability as Diagnostic Biomarkers of Cavernous Angioma with Symptomatic Hemorrhage. J Cereb Blood Flow Metab 2021; doi: 10.1177/0271678X211020587.
18. Girard R, Zeineddine HA, Koskimaki J, et al. Plasma biomarkers of inflammation and angiogenesis predict cerebral cavernous malformation symptomatic hemorrhage or lesional growth. Circ Res 2018;122:1716–1721. [PubMed: 29720384]
19. de Champfleur NM, Langlois C, Ankenbrandt WJ, et al. Magnetic resonance imaging evaluation of cerebral cavernous malformations with susceptibility-weighted imaging. Neurosurgery 2011;68:641–647; discussion 647–648. [PubMed: 21164377]
20. Al-Shahi Salman R, Berg MJ, Morrison L, Awad IA, Angioma Alliance Scientific Advisory Board. Hemorrhage from cavernous malformations of the brain: definition and reporting standards. Angioma Alliance Scientific Advisory Board. Stroke 2008;39:3222–3230. [PubMed: 18974380]
21. Larsson HB, Hansen AE, Berg HK, Rostrup E, Haraldseth O. Dynamic contrast-enhanced quantitative perfusion measurement of the brain using T1-weighted MRI at 3T. J Magn Reson Imaging 2008;27:754–762. [PubMed: 18383268]
22. Larsson HB, Courivaud F, Rostrup E, Hansen AE. Measurement of brain perfusion, blood volume, and blood-brain barrier permeability, using dynamic contrast-enhanced T(1)-weighted MRI at 3 tesla. Magn Reson Med 2009;62:1270–1281. [PubMed: 19780145]
23. McFadden DL. Quantitative Methods for Analyzing Travel Behaviour of Individuals: Some Recent Developments. In: Hensher D, Stopher P, editors. Behavioural Travel Modelling. London, U.K.: Croom Helm; 1977. p. 279–318.
24. Schwarz G. Estimating the dimension of a model. Annals of Statistics 1978;6:461–464.
25. Youden WJ. Index for rating diagnostic tests. Cancer 1950;3:32–35. [PubMed: 15405679]

26. DeLong ER, DeLong DM, Clarke-Pearson DL. Comparing the areas under two or more correlated receiver operating characteristic curves: a nonparametric approach. Biometrics 1988;44:837–845. [PubMed: 3203132]
27. Benjamini Y, Hochberg Y. Controlling the False Discovery Rate: A Practical and Powerful Approach to Multiple Testing. Journal of the Royal Statistical Society Series B (Methodological) 1995;57:289–300.
28. Manley BFJ. Randomization, bootstrap, and Monte Carlo methods in biology. London, United Kingdom: Chapman & Hall: 1997.
29. Gomez-Paz S, Salem MM, Maragkos GA, et al. Role of aspirin and statin therapy in patients with cerebral cavernous malformations. J Clin Neurosci 2020;78:246–251. [PubMed: 32340842]
30. Lyne SB, Girard R, Koskimaki J, et al. Biomarkers of cavernous angioma with symptomatic hemorrhage. JCI Insight 2019;4:e128577. doi: 10.1172/jci.insight.128577.
31. Zhang ZG, Zhang L, Jiang Q, et al. VEGF enhances angiogenesis and promotes blood-brain barrier leakage in the ischemic brain. J Clin Invest 2000;106:829–838. [PubMed: 11018070]
32. Ginat DT, Mangla R, Yeaney G, Schaefer PW, Wang H. Correlation between dynamic contrast-enhanced perfusion MRI relative cerebral blood volume and vascular endothelial growth factor expression in meningiomas. Acad Radiol 2012;19:986–990. [PubMed: 22591719]
33. Lopez-Ramirez MA, Pham A, Girard R, et al. Cerebral cavernous malformations form an anticoagulant vascular domain in humans and mice. Blood 2019;133:193–204. [PubMed: 30442679]
34. Girard R, Li Y, Stadnik A, et al. A roadmap for developing plasma diagnostic and prognostic biomarkers of cerebral cavernous angioma with symptomatic hemorrhage (CASH). Neurosurgery 2021;88:686–697. [PubMed: 33469662]
35. Banks WA, Kastin AJ. Differential permeability of the blood-brain barrier to two pancreatic peptides: insulin and amylin. Peptides 1998;19:883–889. [PubMed: 9663454]
36. Parmar C, Grossmann P, Bussink J, Lambin P, Aerts H. Machine Learning methods for Quantitative Radiomic Biomarkers. Sci Rep 2015;5:13087. doi: 10.1038/srep13087. [PubMed: 26278466]
37. Simpraga S, Alvarez-Jimenez R, Mansvelder HD, et al. EEG machine learning for accurate detection of cholinergic intervention and Alzheimer's disease. Sci Rep 2017;7:5775. doi: 10.1038/s41598-017-06165-4. [PubMed: 28720796]
38. Zhu G, Jiang B, Tong L, Xie Y, Zaharchuk G, Wintermark M. Applications of deep learning to neuro-imaging techniques. Front Neurol 2019;10:869. doi: 10.3389/fneur.2019.00869. [PubMed: 31474928]

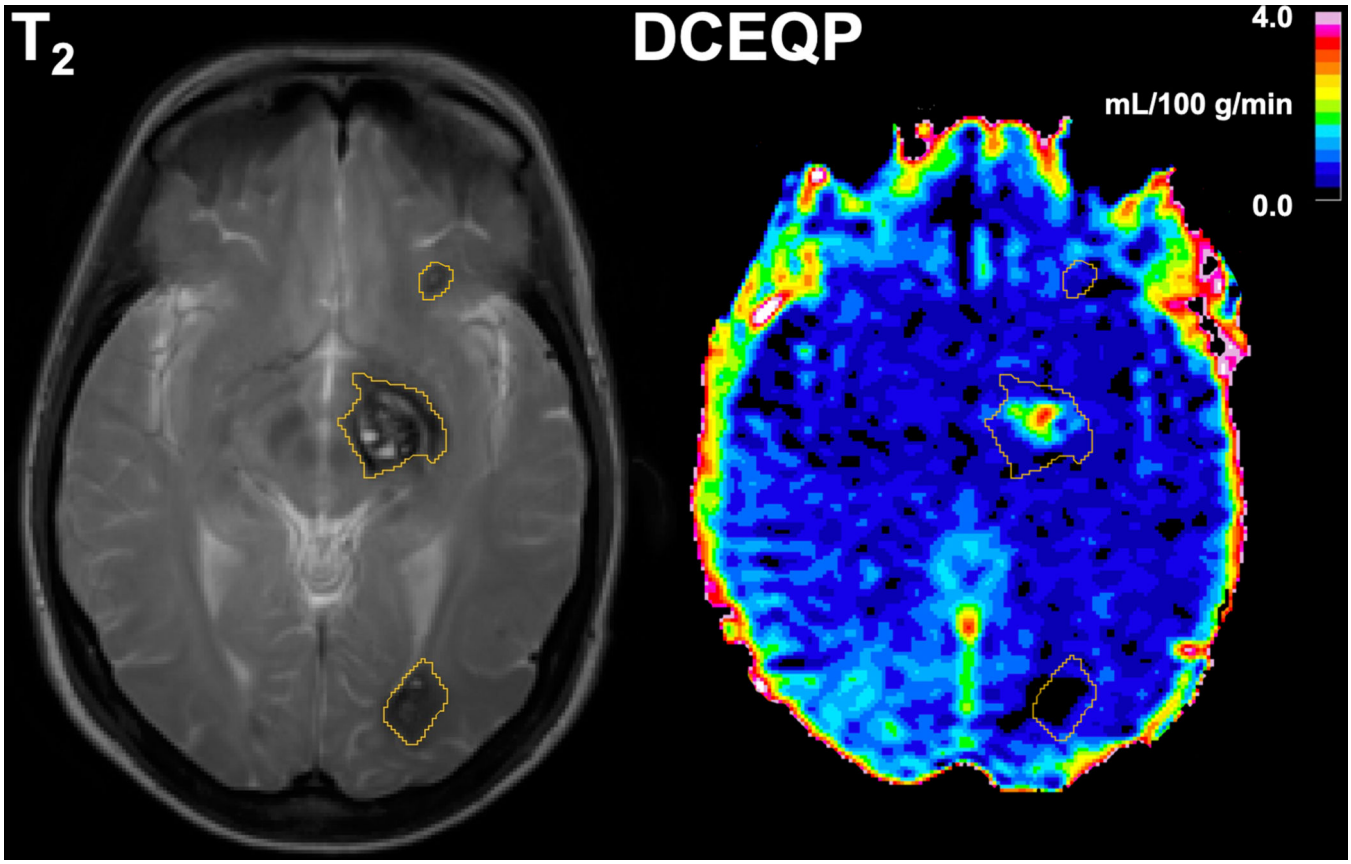

Figure 1: Axial 3.0-Tesla T_2- (left panel) and T_1-weighted dynamic contrast-enhanced quantitative permeability and perfusion (DCEQP, right panel) magnetic resonance (MR) imaging scans with segmented lesional regions of interest (ROIs).

The MR sequences were acquired in July 2013 from a *CCM1* patient with multifocal cavernous angiomas (CAs) who initially presented with a left thalamic/basal ganglia CA (middle ROI) with symptomatic hemorrhage in 2011. The thalamic/basal ganglia CA demonstrated further lesional growth in a subsequent scan in May 2014 while the other lesions (top and bottom ROIs) remained stable.

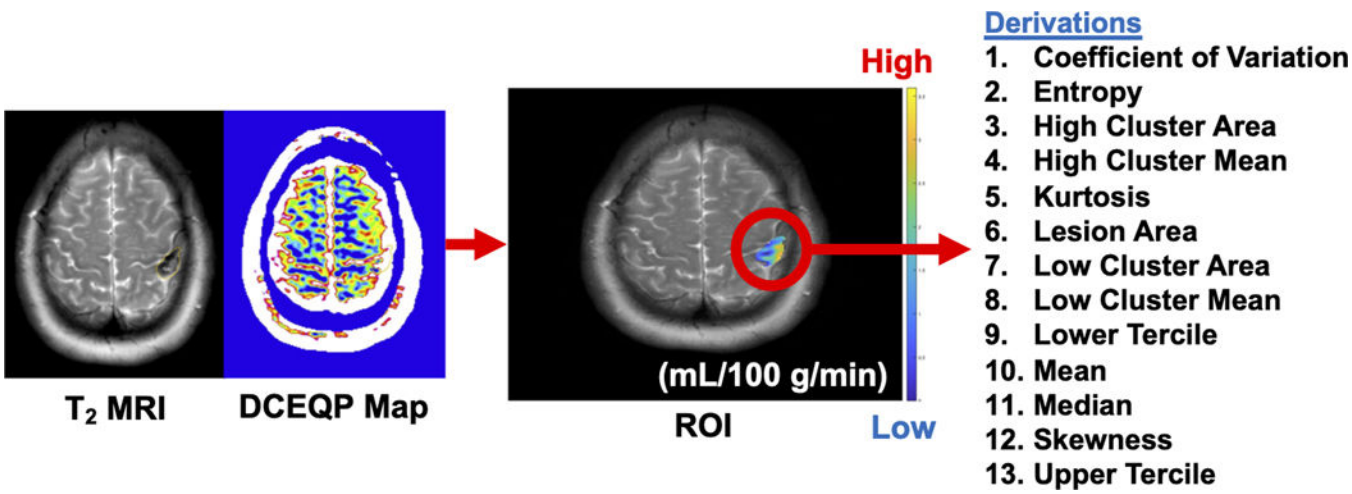

Figure 2: Schematic diagram of dynamic contrast-enhanced quantitative perfusion (DCEQP) map acquisition, imaging postprocessing, and calculation of the 13 respective vascular perfusion and permeability descriptors using MATLAB.

ROI: region of interest.

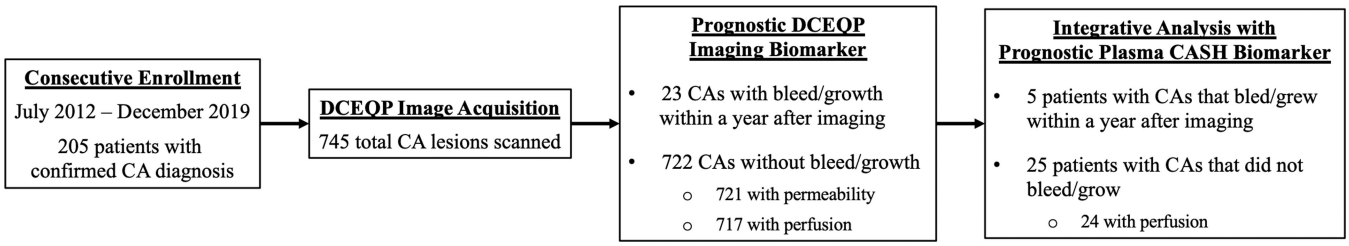

Figure 3: Consort diagram of cavernous angioma (CA) patients and lesions with dynamic contrast-enhanced quantitative perfusion (DCEQP) MRI acquisition.

In 205 patients who were consecutively enrolled during their standard clinical visits, a total of 745 CAs were scanned with DCEQP MRI. There were 23 CAs with bleed/growth within a year after DCEQP imaging. In the subset of CA patients who also had plasma sampled, five had lesional bleed/growth within a year after DCEQP imaging.

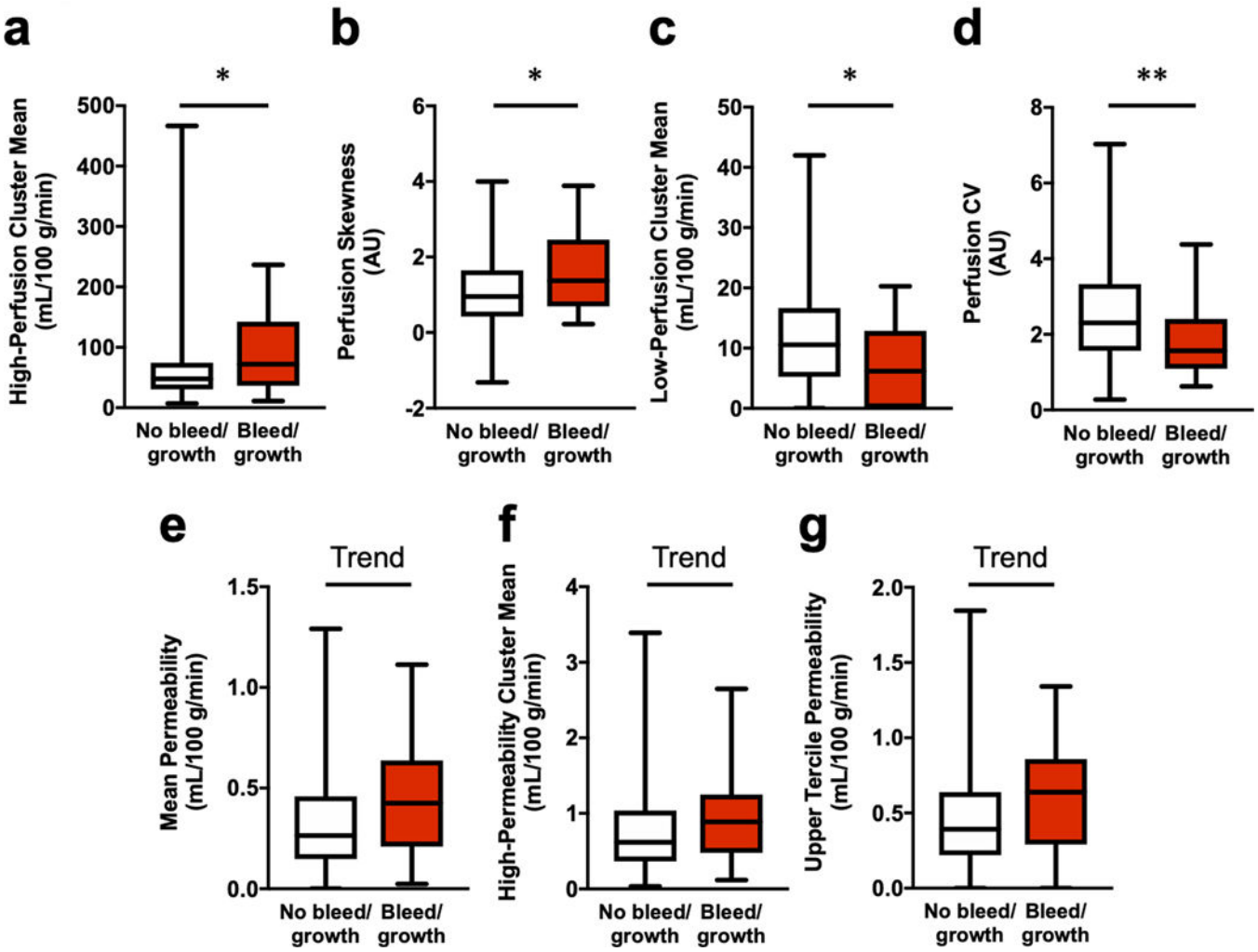

Figure 4: Univariate comparisons of perfusion and permeability descriptors between cavernous angiomas (CAs) with versus without bleed/growth within a year after imaging.

Perfusion (a–d). In CAs with bleed/growth, there were increased median values of **(a)** high-perfusion cluster mean (p=0.029) and **(b)** perfusion skewness (p=0.031), along with decreased **(c)** low-perfusion cluster mean (p=0.021) and **(d)** CV (p=0.004). Permeability (e–g). Additionally, there were higher trends of **(e)** mean permeability (p=0.078), **(f)** upper tercile permeability (p=0.065), and **(g)** high-permeability cluster mean (p=0.063) in CAs with bleed/growth. Boxes represent median and interquartile range. Bars represent range. Outliers with absolute studentized residual values of 3 or greater were excluded. Trend p<0.10, * p<0.05, ** p<0.01. AU: arbitrary unit; CV: coefficient of variation.

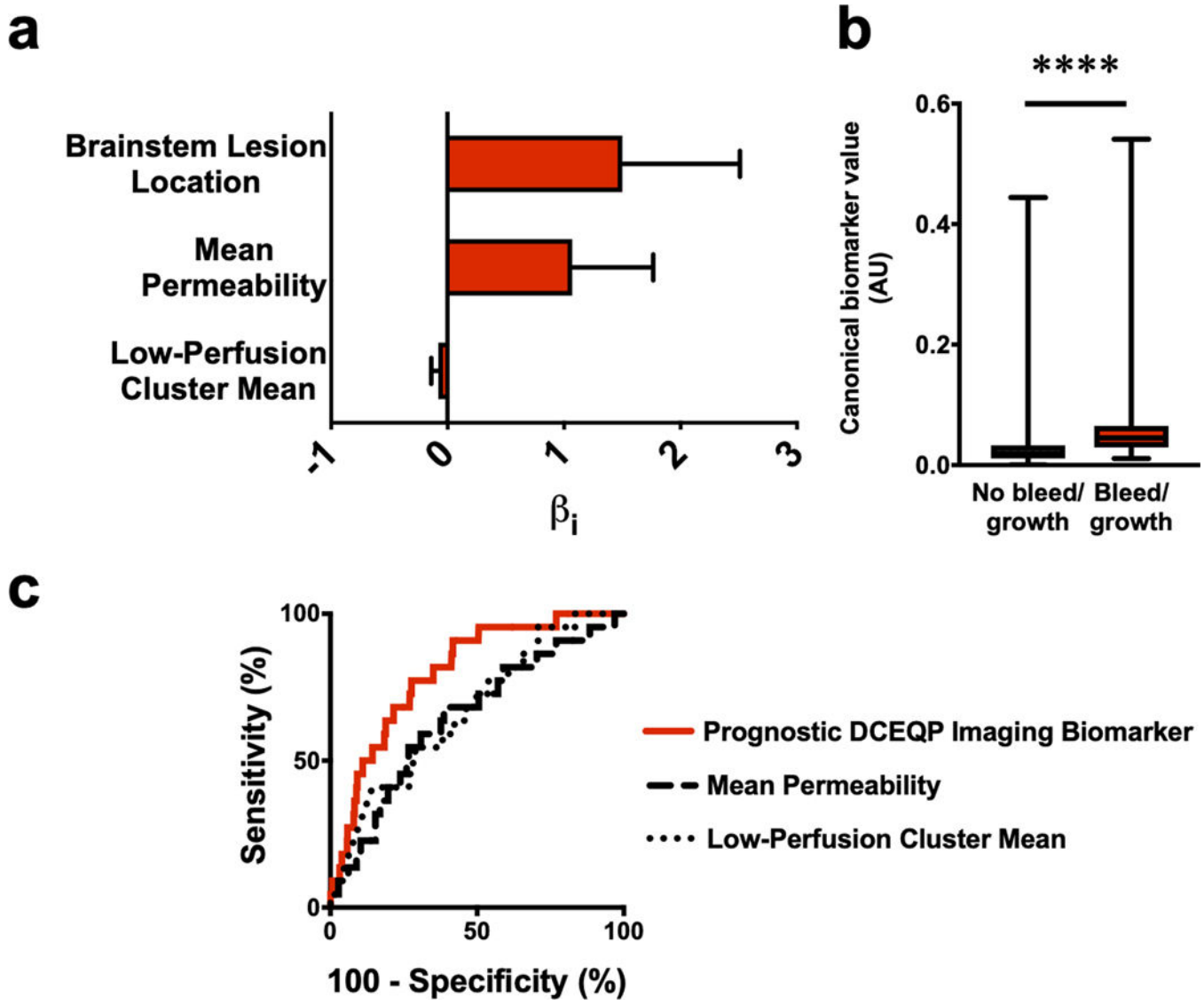

Figure 5: The best prognostic biomarker of cavernous angiomas (CAs) with bleed/growth within a year after imaging.

(a) The weighted β_i coefficients of each covariate in the prognostic biomarker (Bayesian information criterion=201.5, McFadden R^2=0.12); error bars indicate 95% confidence interval (CI). **(b)** Canonical score of the prognostic biomarker was higher (p<0.0001) in CAs with bleed/growth (median [interquartile range]=0.05 [0.03–0.07]) than in CAs with no bleed/growth within a year after imaging (0.02 [0.01–0.03]); boxes represent median and interquartile range, while bars represent range. **(c)** For predicting lesional bleed/growth, the prognostic biomarker (area under the curve [95% CI]=80% [72–88%], p<0.0001) was significantly better (p=0.01, FDR-corrected) than mean permeability (65% [53–76%], p=0.020) or was significantly better (p=0.04, FDR-corrected) than the low-perfusion cluster mean (67% [56–78%], p=0.007) individually. Mean permeability and low-perfusion cluster mean did not significantly outperform each other (p=0.79, FDR-corrected). **** p<0.0001.

AU: arbitrary unit; DCEQP: dynamic contrast-enhanced quantitative perfusion; FDR: false discovery rate.

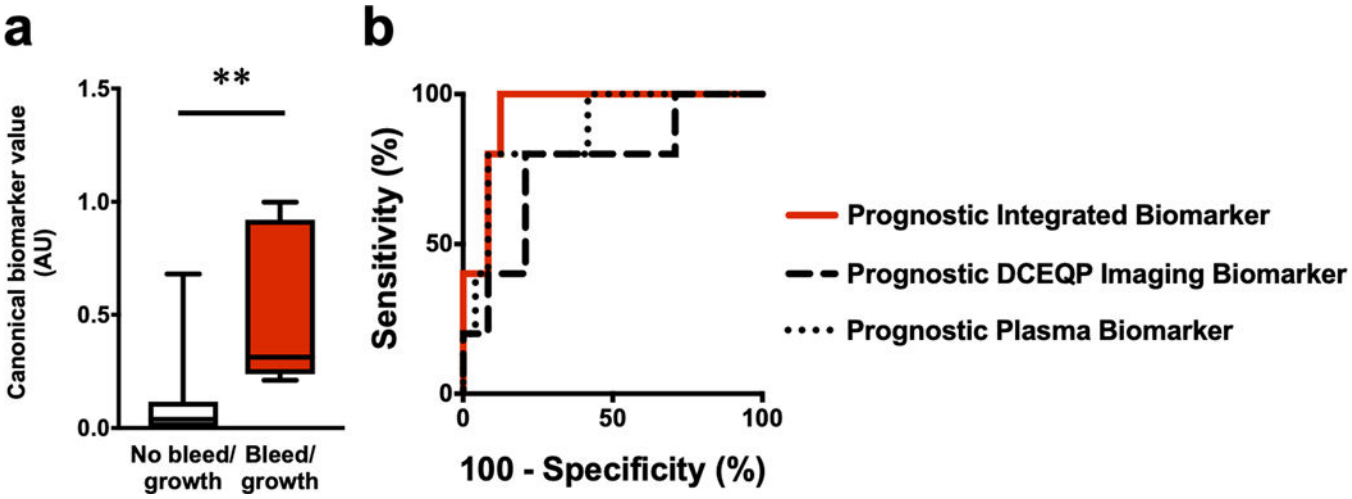

Figure 6: Integrated DCEQP and plasma biomarker of cavernous angioma (CA) with bleed/ growth within a year after imaging.

(a) The canonical score of the integrated prognostic permeability, perfusion, and plasma biomarker was higher (p=0.001) in CA patients with lesional bleed/growth (median [interquartile range] =0.31 [0.24–0.92]) versus those without bleed/growth within a year after imaging (0.04 [0.003–0.12]). **(b)** While the integrated prognostic biomarker (area under the curve (AUC) [95% CI]=94% [86–100%], p=0.002) had higher sensitivity (100%) and specificity (88%) in predicting bleed/growth, this integrated prognostic biomarker did not significantly perform better (p=0.39, FDR-corrected) than DCEQP imaging (80% sensitivity, 79% specificity, AUC=76% [52–100%], p=0.073) and did not significantly perform better (p=0.49, FDR-corrected) than the plasma biomarker individually (80% sensitivity, 92% specificity, AUC=88% [72–100%], p=0.009). The DCEQP imaging and plasma models also did not significantly outperform each other (p=0.49, FDR-corrected). Boxes represent median and interquartile range; bars represent range. ** p<0.01. AU: arbitrary unit; DCEQP: dynamic contrast-enhanced quantitative perfusion; FDR: false discovery rate.

Table 1:

Demographic characteristics of cavernous angioma lesions with versus without bleed/growth within a year after imaging.

Demographics	Lesional bleed/growth (N=23)	No bleed/growth (N=722)	*p*-value
Age, N (%)			0.34 †
< 30 years old	13 (56.5%)	312 (43.2%)	
30 – 50 years old	7 (30.4%)	233 (32.3%)	
> 50 years old	3 (13.0%)	177 (24.5%)	
Female, N (%)	17 (73.9%)	508 (70.4%)	0.82
Ethnicity/race, N (%) *			0.86 †
African American	1 (4.3%)	24 (3.3%)	
Ashkenazi Jewish	0 (0.0%)	7 (1.0%)	
Asian	0 (0.0%)	8 (1.1%)	
Hispanic of Mexican descent	0 (0.0%)	8 (1.1%)	
Hispanic of other descent	0 (0.0%)	34 (4.7%)	
White/Caucasian	22 (95.7%)	627 (87.1%)	
Other	0 (0.0%)	12 (1.7%)	
Sporadic, N (%)	8 (34.8%)	143 (19.8%)	0.11
Familial genotype, N (%)			0.92 †
CCM1	4 (26.7%)	115 (19.9%)	
CCM2	0 (0.0%)	29 (5.0%)	
CCM3	10 (66.7%)	394 (68.0%)	
Multifocal unknown	1 (6.7%)	41 (7.1%)	
Brainstem lesion, N (%)	6 (26.1%)	62 (8.6%)	0.013
Prior symptomatic hemorrhage, N (%)	3 (13.0%)	83 (11.5%)	0.74

* One patient declined to provide information on their ethnicity/race.

† The *p*-values for age, ethnicity/race, and familial genotype refer to overall comparisons and not individual differences among subgroups.